Eur. Phys. J. B **8**, 31–41 (1999)

THE EUROPEAN PHYSICAL JOURNAL B

EDP Sciences

Evolution of charge ordering in $Ca_{1-x}Sm_xMnO_3$ manganites ($0.15 \leq x \leq 0.60$)

M. Hervieu[a], A. Barnabé, C. Martin, A. Maignan, F. Damay and B. Raveau

Laboratoire CRISMAT[b], ISMRA et Université de Caen, 6 Boulevard du Maréchal Juin, 14050 Caen Cedex, France

Received 17 June 1998

Abstract. Charge ordering phenomena in the manganites $Ca_{1-x}Sm_xMnO_3$ have been studied for $0.15 \leq x \leq 0.60$, using electron diffraction and lattice imaging, completed by magnetic and transport measurements. Three domains can be distinguished, depending on the nature of the structural transitions with temperature. For $0.15 \leq x < 0.25$, the structural transition from a pseudo-tetragonal to a monoclinic form, with decreasing temperature, coincides with the competition between ferromagnetism and antiferromagnetism that is characterized by the temperature T_{peak} on the $M(T)$ curves; short-range charge ordering is observed for $0.20 \leq x < 0.25$ manganites. For the second domain, $0.25 \leq x \leq 0.50$, a structural transition from an orthorhombic to a long-range charge ordered state is clearly observed with decreasing temperature. The corresponding temperature T_{CO} coincides with the temperature T_{peak} deduced from magnetic measurements. This long range charge ordering, which appears along **a**, is either commensurate or incommensurate depending on the x value, with a modulation qa^* vector, q being close to x. These modulated superstructures correspond to a stacking of single Mn^{3+} stripes with multiple Mn^{4+} stripes along **a**, either in a commensurate or in an incommensurate manner. The third domain $0.50 < x \leq 0.60$, is characterized by a transition to a charge ordered state with commensurate superstructure at low temperature. The latter can be described as a "partially" charge ordered state in which single "Mn^{3+}" stripes alternate with mixed "Mn^{3+}/Mn^{4+}" stripes.

PACS. 61.14.-x Electron diffraction and scattering – 75.30.-m Intrinsic properties of magnetically ordered materials – 72.20.My Galvanomagnetic and other magnetotransport effects

1 Introduction

The investigations carried out recently on colossal magnetoresistive (CMR) manganites have shown that the transport and magnetic properties of these oxides are strongly correlated to the appearance or disappearance of charge ordering (CO) phenomena. In manganites, the CO state corresponds to the ordering of Mn^{3+} and Mn^{4+} species in the perovskite matrix. It generally appears for different Mn^{3+}/Mn^{4+} ratios, compatible with the periodicity of the crystal lattice, as shown for instance for $Pr_{1-x}Ca_xMnO_3$ [1,2]. Although it is expected to be optimized for a commensurate order of the Mn^{3+} and Mn^{4+} species, corresponding for instance to $x = 1/2$, charge ordering can extend to x values far away from 1/2 (*e.g.* $x \cong 0.30$, leading to an incommensurate ordering). The strong coupling between the charge carriers and spins, according to the double exchange theory [3–5], makes that the CMR properties of the manganites are highly influenced by CO. This is illustrated by the magnetic field induced metal-insulator transition in the $Pr_{1-x}Ca_xMnO_3$ system, for which Tomioka *et al.* [6] have demonstrated that this transition results from the melting of the insulating CO state, itself favored by a deviation of x from the ideal $x = 1/2$ value.

The nature of charge ordering, and its evolution *versus* temperature, are so far not fully understood due to the small number of investigations that have been performed to date on manganites. In this respect, the electron microscopy study of $La_{0.50}Ca_{0.50}MnO_3$ by Chen *et al.* [7] is of great interest, since it shows that the commensurability of the CO structure, characterized by the qa^* vector, varies progressively during the transition, from an incommensurate state ($q \approx 0.4$) below 240 K to a quasi commensurate one ($q \approx 1/2$) at low temperature. A similar behavior has recently been observed for $Sm_{0.50}Ca_{0.50}MnO_3$ [8].

Electron microscopy investigations of CO phenomena have been performed for the half doped manganites $Ln_{0.50}Ca_{0.50}MnO_3$, Ln = La, Pr, Nd, Sm, Eu and Gd [7,8,23] but also for different Mn^{3+}/Mn^{4+} ratios, as in $La_{1-x}Ca_xMnO_3$ [10–12], in $Nd_{1-x}Ca_xMnO_3$ [13,14] and in the Mn^{IV} rich systems [15–17]. The recent discovery of CMR effect in electron doped manganites, $Ca_{1-x}Ln_xMnO_3$ with $x < 0.50$ [17–21], sets the problem of the nature of charge ordering and of its evolution as

[a] e-mail: hervieu@crismat.ismra.fr
[b] CNRS – UMR 6508

the electron concentration increases, as it has been already emphasized in the $Ca_{1-x}Sm_xMn_{1-y}Cr_yO_3$ system [22].

In this study, we investigate the charge ordering phenomena *versus* temperature in the manganites $Ca_{1-x}Sm_xMnO_3$ for x ranging from 0.15 to 0.60, using electron microscopy. We show that the magnetic and transport anomalies observed on the $\rho(T)$ and $M(T)$ curves are systematically correlated to a structural transition. We demonstrate that three domains can be distinguished depending on the composition range. The first one, which appears for $0.15 \leq x < 0.25$, corresponds to compounds exhibiting a transition from a pseudo-tetragonal to a monoclinic phase as T decreases, and includes the area where CMR properties are observed ($x < 0.20$). The second domain which exists for $0.25 \leq x \leq 0.50$ corresponds to compounds showing a transition from an orthorhombic phase to a charge ordered state at low temperature, the latter involving modulated superstructures with q factors equal to x, continuously from $q = 1/4$ to $q = 1/2$. In the third domain, $0.50 < x \leq 0.60$, charge ordering is also observed, but the structure remains commensurate with $q = 1/2$, whatever x.

2 Experimental

Polycrystalline samples were synthesized from stoichiometric mixtures of Sm_2O_3, CaO and MnO_2, according to the experimental method previously described [19–21]. The mixtures with nominal compositions $Ca_{1-x}Sm_xMnO_3$ ($0.15 \leq x \leq 0.60$) were first heated at 1000 °C, sintered at 1200 °C and then at 1500 °C for 12 hours and slowly cooled down to room temperature.

The structural characterizations and physical properties measurements reported herein were carried out on the as-synthesized samples. It is indeed necessary to bear in mind that oxygen stoichiometry is also a factor influencing the CO state [23].

The electron diffraction (ED) study at room temperature was performed with a JEOL 200Cx electron microscope fitted with a tilting-rotating sample holder (tilt $\pm$ 60° and rotation $\pm$ 180°). The ED study *versus* temperature and the bright/dark field imaging were carried out with a JEOL 2010 electron microscope fitted with a double tilt cooling sample holder ($\pm$ 40° for 92 K $\leq T \leq$ 300 K). The ED patterns were recorded *versus* T keeping a constant electron current density. For the different samples, experiments with long irradiation times were carried out to check a possible influence of the electron irradiation on the different phenomenon which have been observed. In the present samples, no significant effect were detected. The positions of the spots in electron diffraction patterns were measured from films by using video processor TAMRON Fotovix II x-S. This CDD image has a 470 000 pixels high resolution for a 6 times maximum enlarging. Each value corresponds to a minimum of 10 average measurements in the ED patterns, without any important standard deviation. All the scans were carried out following the same experimental conditions, *i.e.*, increasing the temperature from 92 K to 300 K, waiting for the temperature stabilization before each ED recording, made with a constant electron beam adjustment. For the "limit" ED patterns, for which the existence or absence of extra reflections is in the limit of detection, several exposure times were used.

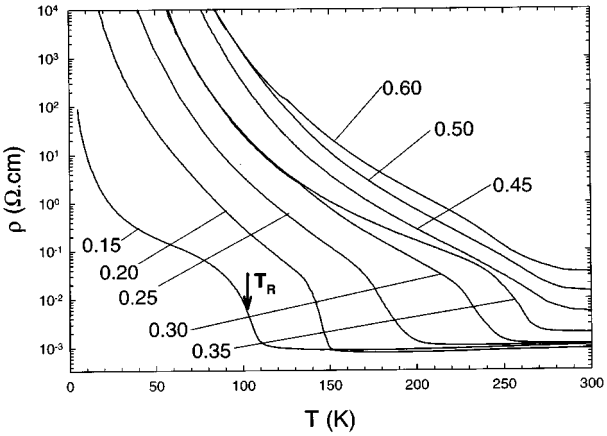

Fig. 1. T dependence of the resistivity for the $Ca_{1-x}Sm_xMnO_3$ samples with $0.15 \leq x \leq 0.60$ (x values are labelled on the graph). The arrow indicates T_R.

The high resolution electron microscopy (HREM) study was made with a TOPCON 002B electron microscope operating at 200 kV (Cs = 0.4 mm). The microscopes are equipped with KEVEX analysers. For each of the samples, energy dispersive spectroscopy (EDS) analyses were systematically performed on numerous grains.

The powder X-ray diffraction (XRD) data were collected with a Philips diffractometer (CuKα radiation) in the range $10° \leq 2\Theta \leq 110°$ by increment of 0.02° (2Θ).

The resistivity measurements were performed from room temperature down to 5 K, by the four probe method on sintered bars, in the earth magnetic field or in 7 T. The magnetization *versus* temperature was registered on warming with a vibrating sample magnetometer in a magnetic field of 1.4 T, which was applied at 4.2 K after a zero field cooling.

3 Results and discussion

3.1 Magnetic and transport properties of $Ca_{1-x}Sm_xMnO_3$

The magnetic and transport properties of the manganites $Ca_{1-x}Sm_xMnO_3$ have already been published for $0 \leq x \leq 0.20$ [19–21]. These previous results, completed by new data corresponding to the composition range $0.20 < x \leq 0.60$, are given in Figures 1 and 2. For $0.15 \leq x \leq 0.60$, the $\rho(T)$ curves (Fig. 1) show a transition from a semimetallic or semiconducting state to an insulating state as T decreases. The corresponding transition temperature, T_R, which corresponds to the inflexion point of the curve, is indicated by an arrow in Figure 1.

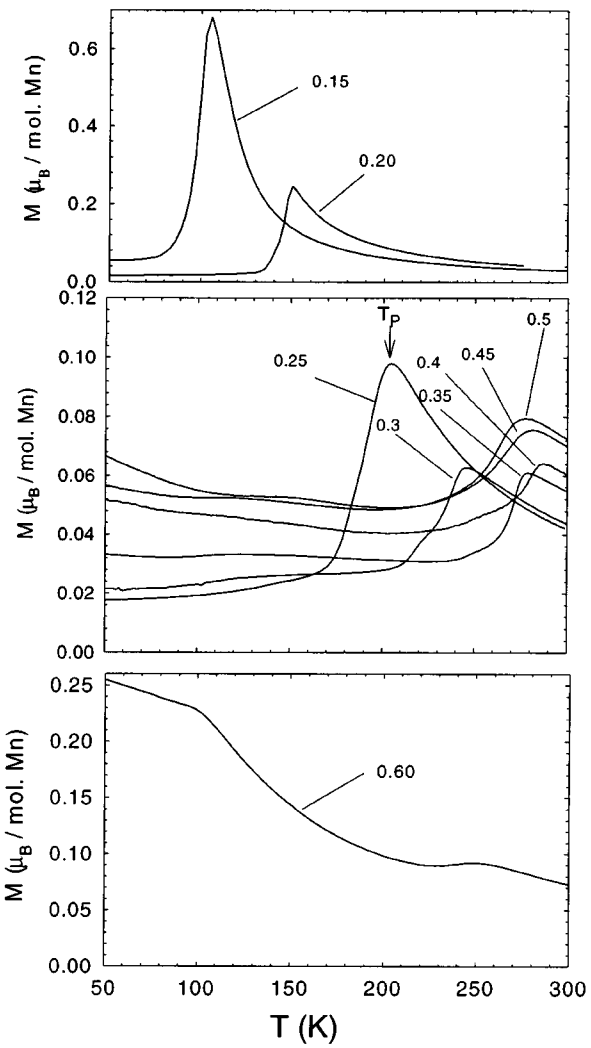

Fig. 2. T dependence of the magnetization of the series $Ca_{1-x}Sm_xMnO_3$ samples where T_{peak} indicates the temperature of the maximum magnetization value.

This resistive transition, already observed for other manganites [6], is commonly attributed to charge ordering phenomena. Concomitantly, the $M(T)$ curves (Fig. 2) show a peak whose temperature T_{peak} coincides with T_R, confirming the strong interplay between magnetic and transport properties, since the magnetization decrease observed below T_{peak} is related to the antiferromagnetic ordering – hence localization – of Mn^{3+} and Mn^{4+} charges. From these $M(T)$ curves, it must be emphasized that T_{peak} does not evolve regularly with x in $Ca_{1-x}Sm_xMnO_3$ for x values ranging from 0.15 to 0.60 (Fig. 3). T_{peak} is maximum for $x = 0.40$, so that T_{peak} first increases from 110 K for 0.15 to 285 K for $x = 0.40$, and then decreases from 285 K to 240 K for $x = 0.60$. Moreover, the M value at T_{peak} is severely reduced as x increases from 0.15 to 0.25 and then keeps rather similar values beyond this value. This suggests that the strong competition existing between ferromagnetic and antiferromagnetic interactions in $Ca_{0.85}Sm_{0.15}MnO_3$ ($x = 0.15$), which is responsible for the CMR observed at this peculiar composition [19,20],

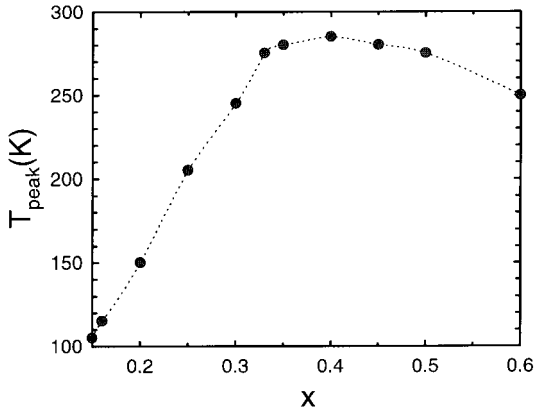

Fig. 3. x dependence of T_{peak} (the dotted line is only a guide to the eye). (note that T_{peak} coincides with T_R).

tends to decrease as x increases from $x = 0.15$, because of the strong reduction of the ferromagnetic interactions in agreement with the antiferromagnetic interactions development.

This is corroborated by the magnetoresistance properties shown in Figure 4 for $x = 0.15$, $x = 0.20$ and $x = 0.60$. In contrast to the $x = 0.15$ compound, CMR properties are not observed for $0.20 \leq x \leq 0.60$. All these results strongly suggest that CO, if it exists, changes of nature in the $x = 0.15$–0.25 domain. Moreover, the lack of CMR properties of $Ca_{0.40}Sm_{0.60}MnO_3$ in comparison with the $Ca_{0.40}Pr_{0.60}MnO_3$ compound [6] emphasizes that it is of capital importance to study accurately the evolution of CO *versus* temperature, from $0.15 \leq x \leq 0.60$ using electron microscopy.

3.2 Preliminary characterizations of the room temperature Pnma structure

The systematic investigation of the oxides $Ca_{1-x}Sm_xMnO_3$, for $0.15 \leq x \leq 0.60$, using both XRD and ED shows that they are single phased, with an orthorhombic $GdFeO_3$-type cell, $a = a_p\sqrt{2}$, $b = 2a_p$ and $c = a_p\sqrt{2}$, space group $Pnma$, at room temperature (a_p is the parameter of the cubic perovskite subcell). The EDS analyses confirm their great homogeneity, with a cationic composition identical to the nominal one "$Ca_{1-x}Sm_xMn_1$", in the limit of the experimental error. The cell parameters, refined from XRD data in the $Pnma$ space group, increase as x increases, in agreement with the increase of Mn^{3+} content (Fig. 5). Although the cell volume increases regularly with x, the evolution of the lattice parameters is more complex. Starting from the smallest x values the cell is first pseudo-tetragonal ($a = 5.3166(2)$ Å, $b = 7.4922(2)$ Å and $c = 5.2968(2)$ Å for $x = 0.16$) and then the orthorhombic distortion increases with x($a = 5.4603(2)$ Å, $b = 7.5675(2)$ Å and $c = 5.3688(2)$ Å for $x = 0.60$ for instance).

The HREM performed on each of these compounds confirms the high quality of their crystallization. The comparison of the experimental HREM images with those calculated from positional parameters deduced from XRD

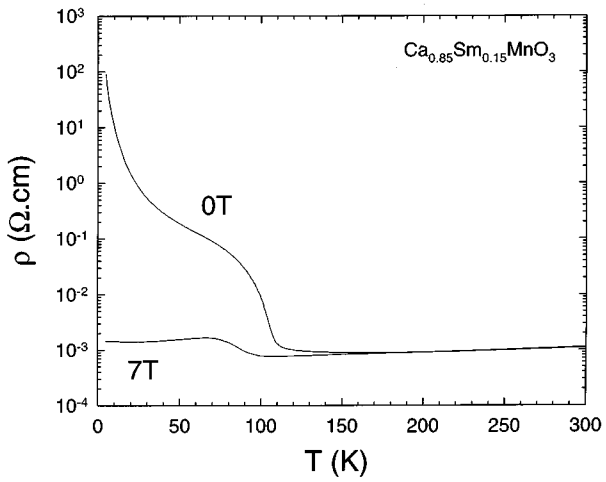

(a)

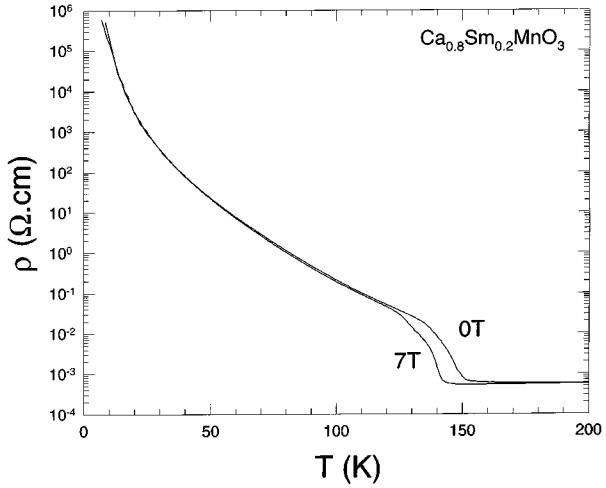

(b)

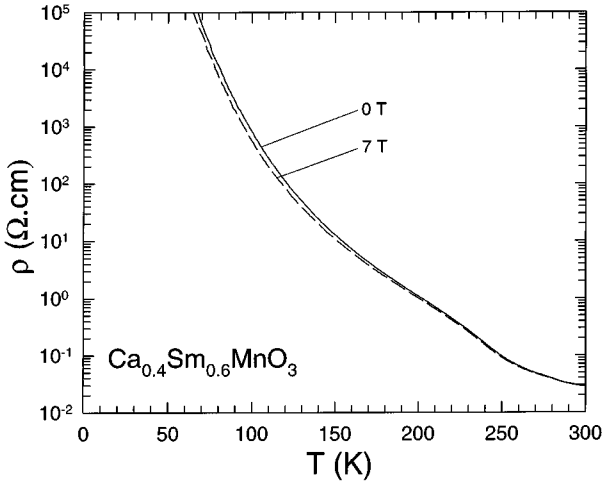

(c)

Fig. 4. T dependence of the resistivity registered in 0 and 7 T for three $Ca_{1-x}Sm_xMnO_3$ compounds corresponding to $x = 0.15$ (a), $x = 0.20$ (b) and $x = 0.60$ (c).

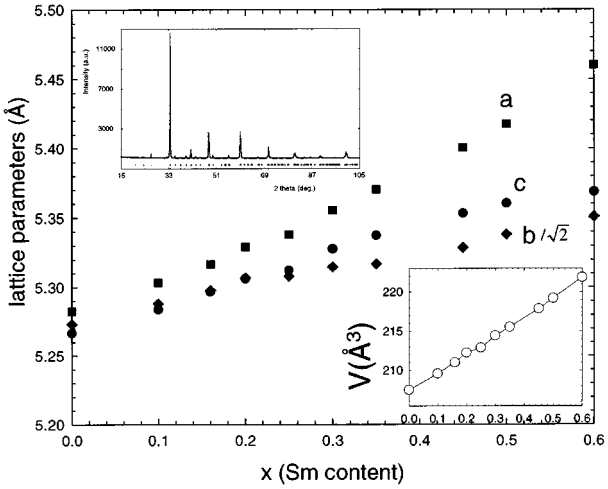

Fig. 5. Evolution of the parameters of the *Pnma*-type orthorhombic cell, at room temperature, *versus* Sm content (x ranging from 0 to 0.60). Insets: evolution of the cell volume *versus* x and refined X-ray pattern for $Ca_{0.70}Sm_{0.30}MnO_3$.

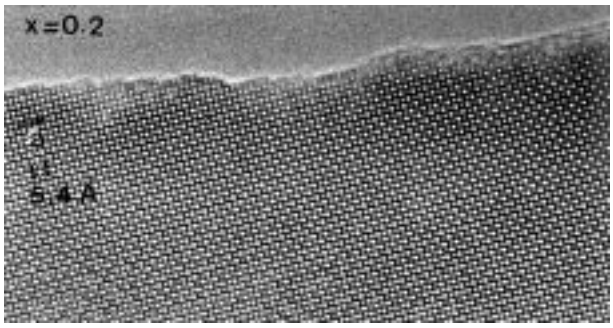

Fig. 6. Typical [010] HREM image of the $Ca_{0.8}Sm_{0.2}MnO_3$ crystallites. A very uniform contrast is commonly observed.

refinements shows a good fit. A [010] HREM, typical of the $Ca_{0.8}Sm_{0.2}MnO_3$ crystallites, is given in Figure 6, illustrating the very even contrast observed in this material. Note that, contrary to $x \leq 0.2$ samples, the [010] HREM images recorded for the high Sm content, namely $0.30 \leq x \leq 0.50$, show the existence of "point like" defects. Such defects were also observed in $Sm_{0.5}Ca_{0.5}MnO_3$ [8] and other $Ln_{0.5}Ca_{0.5}MnO_3$ [23] as well as in $Pr_{0.7}A_{0.3}MnO_3$ [24]. Their presence was associated with the local formation of $AMn^{IV}O_3$ clusters. Lastly, 90° oriented domains are commonly observed in these materials; they result from the orthorhombic distortion of the perovskite cell and have been reported in most of the $Ln_{1-x}A_xMnO_3$ manganites [8,14,24].

3.3 $0.15 \leq x < 0.25$: a monoclinic form at low temperature

The ED study carried out from 92 K to room temperature shows that the system of intense Bragg reflections is kept in the whole temperature range and is similar to that of the room temperature *Pnma* structure. At 92 K, the cell parameters remain unchanged with respect to the *Pnma*

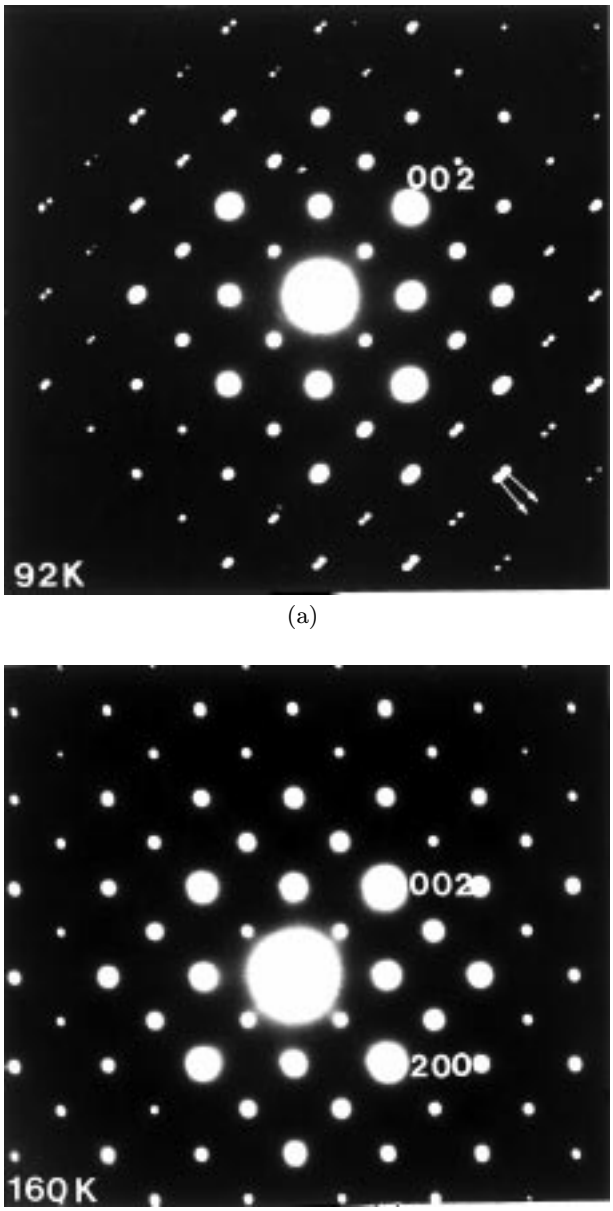

(a)

(b)

Fig. 7. $Ca_{0.80}Sm_{0.20}MnO_3$: [010] ED pattern recorded at (a) 92 K, (b) 160 K.

structure, ($a \cong a_p\sqrt{2}$, $b \cong 2a_p$, $c \cong a_p\sqrt{2}$), but a strong monoclinic distortion is evidenced as shown from the [010] ED pattern of the $x = 0.20$ sample, which exhibits a splitting of the $h00$ reflections (Fig. 7a). The corresponding bright field images (Fig. 8a) show the formation of twinning domains which result from this monoclinic distortion. The twin boundaries are parallel to (001). For $x = 0.20$ an abrupt transition at 155 K appears as T increases, characterized by the disappearance of the splitting of the reflections (Fig. 7b) and concomitantly by the removal of the twinning domains (Fig. 8b), leading to the orthorhombic *Pnma* structure. It is remarkable that this structural transition coincides with the resistive and magnetic

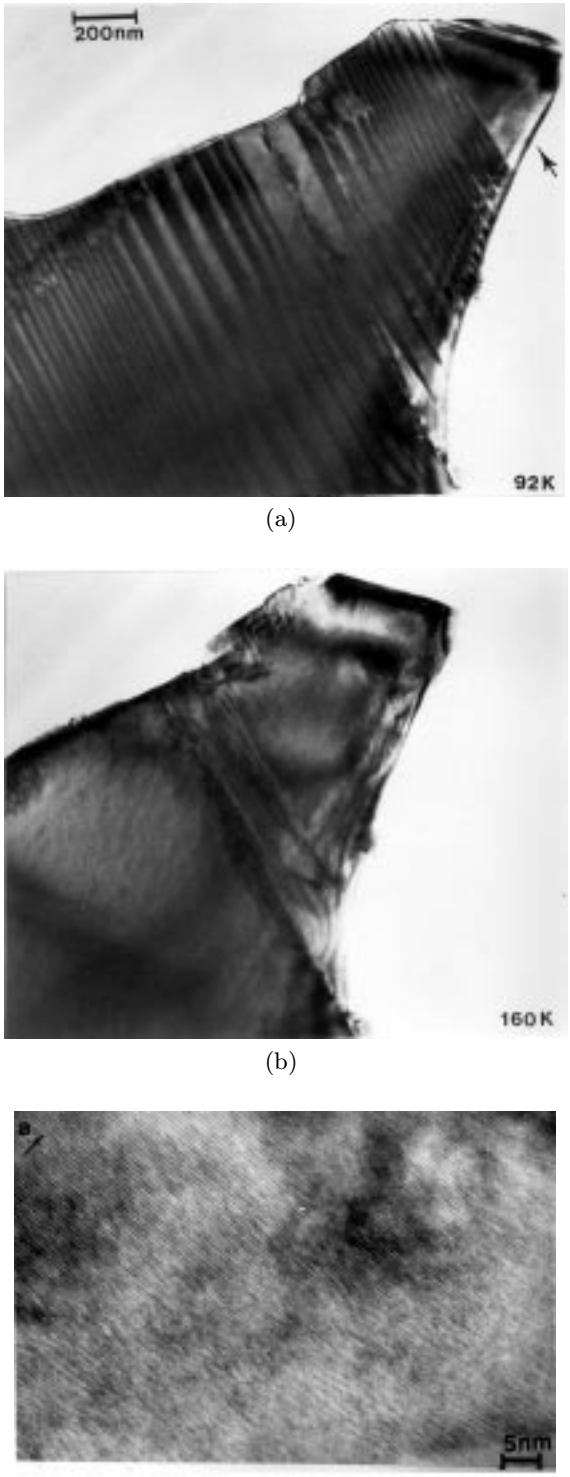

(a)

(b)

(c)

Fig. 8. $Ca_{0.80}Sm_{0.20}MnO_3$: [010] bright field images recorded (a) at 92 K, showing twinning domains (TD) with average width ranging between 10 and 30 nm. The black arrow in the right part indicates an abnormally wide domain; (b) at 160 K. The TD have disappeared but a tweed structure still persists; (c) enlargement of the wide domain indicated by a black arrow in (a), at 92 K. The lattice image shows local variations of the fringes brightness.

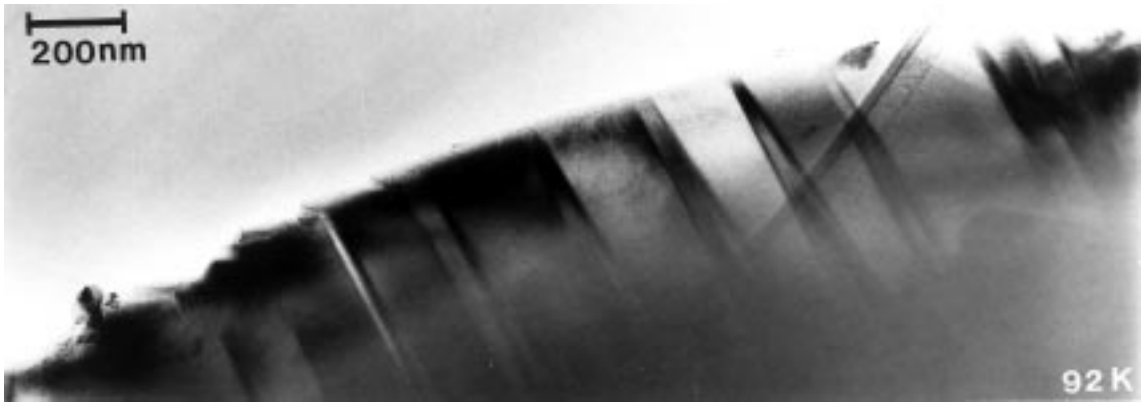

(a)

(b)

Fig. 9. $Ca_{0.85}Sm_{0.15}MnO_3$. [010] Bright field images at (a) 92 K, showing twinning domains and (b) at 120 K.

transitions (Figs. 1, 2), at $T_R \cong T_{peak} \cong 150$ K. This correlation between the structural and physical transitions is confirmed, if one considers the $x = 0.15$ sample, whose twinning domains observed at 92 K (Fig. 9a) disappear at 110 K (Fig. 9b) close to $T_R \cong T_{peak} \cong 105$ K (Figs. 1, 2).

The detailed analysis of the bright field images shows several other important features. The first one deals with the fact that the width of the twinning domains is larger for $x = 0.15$ (Fig. 9a) than for $x = 0.20$ (Fig. 8a), with average values of 70 nm and 10 to 30 nm respectively. The second point concerns the observation, within the twinning domain, of a diffraction contrast effect, commonly called a "tweed" structure. In the electron diffraction patterns, it is associated with a tiny diffuse scattering on the Bragg spots, in the form of small crosses with arms in the $[101]_p$ directions. The tweed structure is systematically observed in the $x \approx 0.20$ crystallites (Fig. 8). It still persists above $T_{peak} = T_R$ whereas the twinning has disappeared, as shown in the bright field image (Fig. 8b), recorded at 160 K for $x = 0.20$. It vanishes slowly at increasing temperature without any clear transition. The tweed structures are often observed during initial stages of a system transformation. In the $Ca_{1-x}Sm_xMnO_3$ system, the observation of the different x samples, shows that, considered separately, the two kinds of structural transitions, monoclinic to orthorhombic ($x = 0.15$) and charge ordered to orthorhombic ($x = 0.2$) do not induce such a tweed texture. However, the tweed structure shows clear orientation relationships with both the twin structure and the short range ordering phenomena at low temperature (see below for $0.2 \leq x < 0.25$). Thus, this suggests that the strain contrast could be associated to the coexistence of the twinning and charge ordering phenomena.

Another feature is also of interest for the understanding of charge ordering phenomena in these oxides, which deals with a modulated contrast observed within the twinning domains of the $0.2 \leq x < 0.25$ samples. Considering the [010] bright field images of $x = 0.20$ sample at low temperature (92 K, Fig. 8a) it can be seen that, from place to place, there exist some domains which exhibit an abnormal width with regard to the average value (black arrow in the right part of the image). The contrast of the lattice images recorded within these large domains (Fig. 8c) consists in fringes which are about 5.5 Å spaced, as expected for the periodicity along **a** but the brightness of the fringes is not regular involving local higher periodicities ($na_p\sqrt{2}$ with $n > 1$). It varies along

the modulation direction **a**, but also along **c**, since it only takes place over a few nanometers. Consequently, this shows that only a short-range ordering appears below $T_{peak} = T_R$ for $0.20 \leq x < 0.25$. This effect could be correlated to the coexistence of ferromagnetic and antiferromagnetic zones.

3.4 $0.25 \leq x \leq 0.50$: commensurate and incommensurate charge ordered structures

For this composition range, the low temperature ED patterns observed at 92 K show the presence of extra reflections in addition to the system of intense reflections corresponding to the room temperature *Pnma* structure. The charge ordering phenomena take place mainly along **a** and lead to a supercell with the following parameters: $a \cong (1/q)a_p\sqrt{2}$, $b = 2a_p$ and $c \cong a_p\sqrt{2}$. There is no condition limiting the reflections. In this supercell the q value characterizes either the commensurate or incommensurate nature of the charge ordering and is found to be roughly equal to the x value, $q \cong x$, at 92 K. In other words, for this composition range, q is directly linked to the Mn^{3+} content. Thus, for $x = 1/4$, $1/3$ and $1/2$ the [010] ED patterns registered at 92 K (Fig. 10) show a commensurate superstructure with a quadrupling (q =1/4), a tripling (q =1/3) and a doubling (q = 1/2) of the a parameter respectively. In contrast, for intermediate x values, the structure is incommensurate, as shown for instance for $x = 0.45$ (Fig. 11a) for which $q \cong 0.43$ at 92 K. Note that at 92 K, q varies linearly with x (Fig. 12) for integral $1/q$ values ($1/q$ = 2, 3, 4) *i.e.*, for commensurate superstructures, and that a small deviation from the linearity appears for intermediate q values corresponding to the incommensurate structures. This slight deviation might be correlated to the difficulty of stabilizing the intermediate modulated superstructures, as will be discussed further.

The evolution of the q value *versus* temperature, for different x compositions ranging from $x = 0.25$ to $x = 0.50$, is shown in Figure 12. Increasing the temperature from 92 K to room temperature, one observes first at low temperature a plateau corresponding to a maximum q value, which is consistent either with a commensurate or with an incommensurate structure depending on x. Then q decreases abruptly, taking intermediate incommensurate q values, and finally in a last step, the intensity of the satellites decreases, leading to weak diffuse streaks along **a**, so that q is no more measurable. For each x value, the $q(T)$ curves show a stair-like shape with increasing temperature. This behavior might be due to thermal instabilities or kinetics during the cooling and heating of the samples but, another possibility is the stabilization of intermediate orderings, corresponding to particular q values (the so-called "lock-in" of the modulated structures). In fact, this effect characterizes the progressive transition from a CO state to the classical *Pnma* structure.

The comparison of the $q(T)$ (Fig. 12) and $T_{peak}(x)$ curves of Figure 3 shows that for most of the samples the charge ordering temperature T_{CO} deduced from the structural evolution coincides with the temperature T_{peak}. A deviation between the two values is observed for $x = 0.30$ and $x = 0.35$, which correspond to the abrupt part of the $T_{peak}(x)$ curve. Nevertheless, beside the low temperature plateau corresponding to q_{max}, one often observes just below T_{CO} a slight decrease of q as T increases. This phenomenon for $0.25 \leq x \leq 0.30$ and $0.40 \leq x \leq 0.50$ might be due to intermediate orderings.

The lattice images recorded at 92 K for $x = 0.50$, 0.33 and 0.25 confirm that a commensurate structure is observed at low temperature. One of them was previously presented for $x = 0.50$ [8]. These images show a system of fringes spaced by 22 Å for $x = 0.25$ (Fig. 10a), 16.5 Å for $x = 0.33$ (Fig. 10b) and 11 Å for $x = 0.50$ (Fig. 10c), corresponding to a parameters of $4a_p\sqrt{2}$, $3a_p\sqrt{2}$ and $2a_p\sqrt{2}$ respectively. Charge ordering between Mn^{3+} and Mn^{4+} have previously been proposed by several authors to explain similar superstructures in $La_{1-x}Ca_xMnO_3$ oxides [9]. In the present case, the lattice images suggest that these various commensurate superstructures consist in the ordered alternation along **a** of one (100) Mn^{3+} stripe with n Mn^{4+} stripes. It should be recalled that the appearance of fringes in the lattice images, corresponding to the fundamental or superlattice reflecting planes, is of importance for the characterisation of periodic specimens and in the study of the short and long range ordering phenomena but that care must be exercised in the interpretation of the images. This is especially the case of the present materials in which the ordering feature is only generated by MnO_6 octahedra distortions and the small correlated displacements of the surrounding atoms. HREM imaging would therefore be essential to clarify the interpretation. Based on the observed periodicities, several structural models can be proposed. The simplest ones, drawn in Figure 13, correspond to the sequences 1/1, 1/2 and 1/3. Thus, regular n members $(AMn^{IV}O_3)_n(AMn^{III}O_3)_1$, have to be considered, $x = 0.50$ corresponding to $n = 1$ (Fig. 13a), $x = 0.33$ to $n = 2$ (Fig. 13b) and $x = 0.25$ to $n = 3$ (Fig. 13c).

The situation is more complex for the intermediate x samples, as examplified by the two lattice images (Figs. 11b, 11c) recorded for $Ca_{0.55}Sm_{0.45}MnO_3$ crystallites, and characterized by a modulation vector $q = 0.44$ (Fig. 11a):

- A first effect is observed in Figure 11b, where alternating bright and gray fringes are clearly observed in the left part of the image, which reflect the ordered superstructure. However, in the larger part of the crystal, no regular sequence is established (see for example the area indicated by a white arrow). This shows that the ordering takes place throughout the whole matrix but only in a short range manner.
- A second effect is shown in Figure 11c, in a zone where a complex but regular sequence of fringes (bright-gray-bright-gray-bright-gray-gray) is observed, according to the periodicity $a \approx 7a_p\sqrt{2}$. This observation is consistent with the local stabilization of the member $[(AMn^{IV}O_3)(AMn^{III}O_3)]_3(AMn^{IV}O^3)$, corresponding to a theoretical $q = 0.429$ which is close to the experimental one ($q = 0.44$). However, it is clearly observed by viewing Figure 11c at grazing incidence

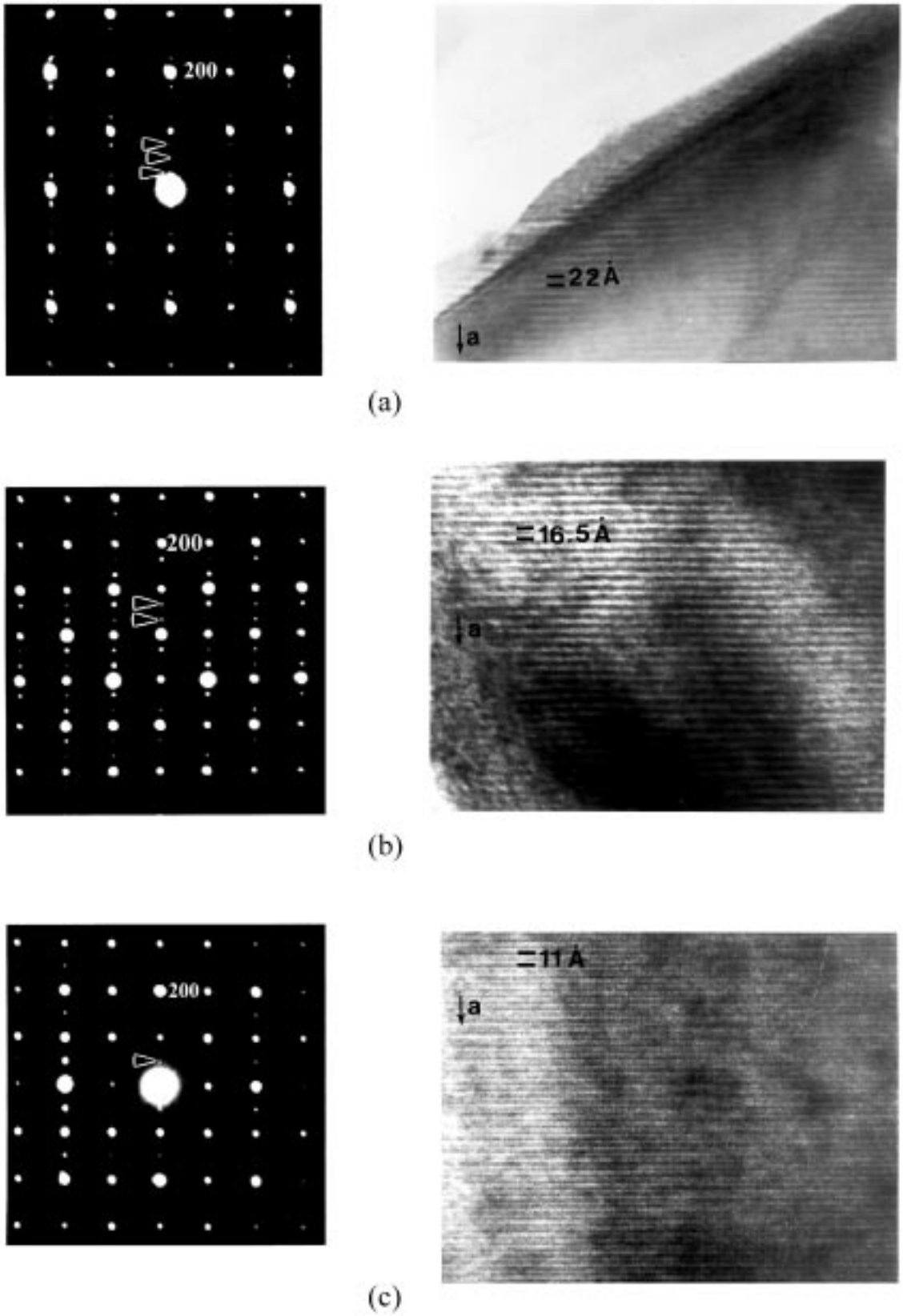

Fig. 10. [010] ED patterns and [010] lattice images recorded at 92 K for: (a) $x = 0.25$ (b) $x = 0.33$ and (c) $x = 0.50$ of the $Ca_{1-x}Sm_xMnO_3$ system.

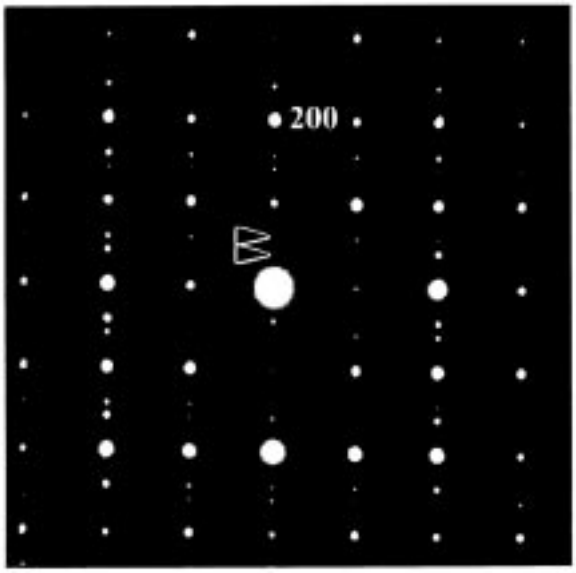

(a)

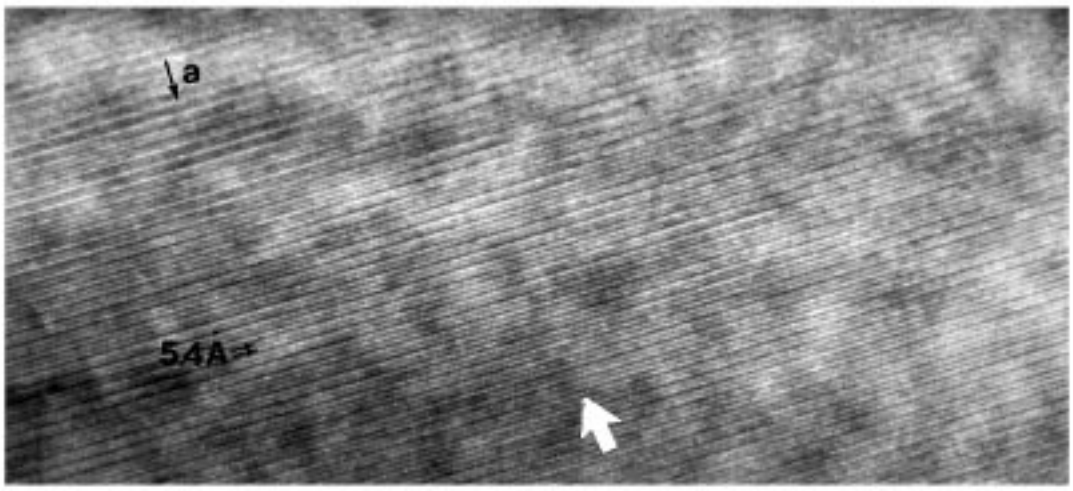

(b)

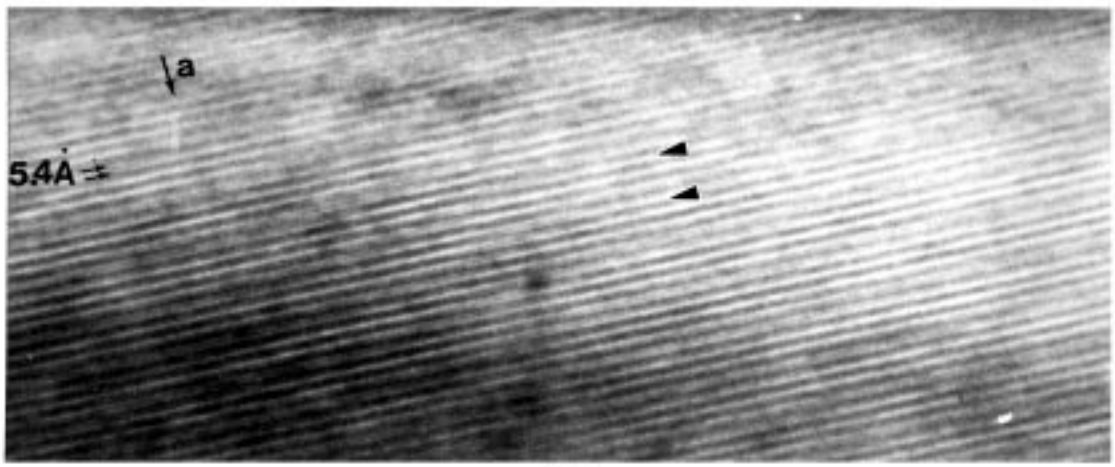

(c)

Fig. 11. $Ca_{0.55}Sm_{0.45}MnO_3$ at 92 K; (a) [010] pattern and [010] lattice images of different areas of the corresponding crystallite. They exemplify (b) short range ordering and (c) long range ordering.

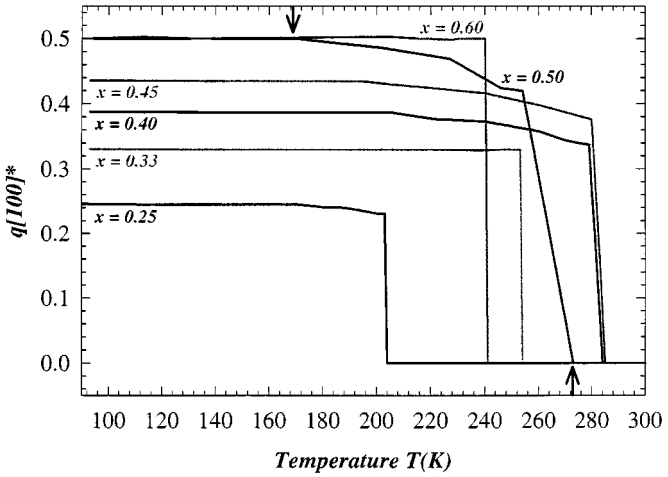

Fig. 12. Evolution of q *versus* T for the different $Ca_{1-x}Sm_xMnO_3$ samples with $0.15 \leq x \leq 0.60$. For the $x = 0.50$ sample, arrows indicate two particular temperatures; ↑: temperature which appears superlattice spot in cooling (T_{CO}); ↓: temperature which the q value remains constant ($q = q_{max}$).

the modulation vector is not strictly parallel to **a** and that a component along **c** exists, due to a shifting, by $a_p\sqrt{2}$, of the modulated contrast. It is worth noting that in all the lattice images recorded for the intermediate q values, there systematically exists shearing mechanisms.

3.5 $0.50 < x \leq 0.60$: commensurate "partially" charge ordered manganites

For $x > 0.50$ up to $x = 0.60$, the ED patterns recorded at 92 K are similar to those of $x = 0.50$, *i.e.*, show a doubling of the a parameter ($q = 1/2$). The commensurate nature of the structure is also confirmed by the lattice images for $x = 0.60$, which are identical to those of $x = 0.50$ (Fig. 10c). The conditions of reflection are $0k0$ $k = 2n$, which are consistent with the $P2_l/m$ space group proposed by Radaelli [25] in $La_{0.50}Ca_{0.50}MnO_3$. Two main differences are characteristic of these compositions with regard to the Ca-rich ones:

- The evolution of the q value with x: q remains constant, whatever x ranging from 0.50 to 0.60 (Fig. 12). The fact that the q value remains equal to 1/2 whatever x suggests that the structure of the phases is derived from that of the $x = 0.50$ manganite by distributing the additional Mn^{3+} species in the Mn^{4+} stripes, statistically, so that for $x = 0.60$, 20% of the Mn^{4+} sites are occupied at random by Mn^{3+}. Thus, the commensurate structure of the latter manganite (Fig. 13a) consists of (100) Mn^{3+} stripes which alternate with "Mn^{4+}/Mn^{3+}" mixed stripes (20% occupied by Mn^{3+}).
- The evolution of q with T: the structural transition as it appears from the evolution of the $q(T)$ curve (Fig. 12) for $x = 0.60$, is abrupt compared to

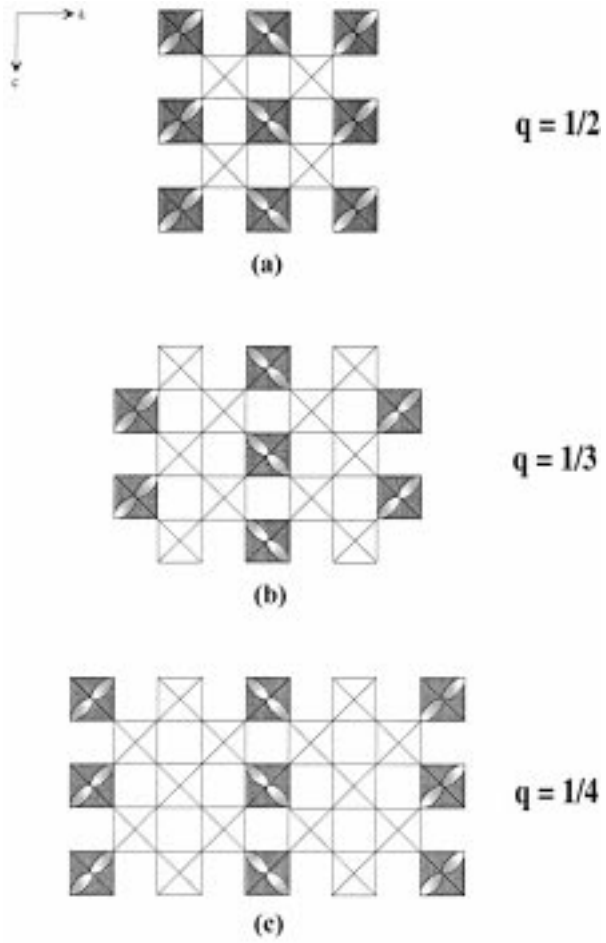

Fig. 13. Example of structural models for $(AMn^{IV}O_3)_n(AMn^{III}O_3)_1$ with $n = 1$ (a), $n = 2$ (b) and $n = 3$ (c).

$x = 0.50$, and does not involve the formation of any intermediate incommensurate structure, contrary to the samples $0.25 \leq x \leq 0.50$.

4 Conclusion

This study shows that the transitions observed on the physical properties of the manganites $Ca_{1-x}Sm_xMnO_3$ ($0.15 \leq x \leq 0.60$) are closely related to structural transitions. The charge ordered state at low temperature depends of the Mn^{4+}/Mn^{3+} content. Only short range ordering is obtained for high Mn^{4+} contents ($0.20 \leq x < 0.25$), whereas a long range modulated charge ordering is obtained for lower Mn^{4+} contents ($0.25 \leq x \leq 0.50$). For $0.50 < x \leq 0.60$, it is remarkable that the Mn^{4+} and Mn^{3+} species tend to form mixed stripes, avoiding the formation of adjacent Mn^{3+} stripes, so that a partial charge ordering is obtained in which one single Mn^{3+} stripe alternates with one mixed Mn^{4+}/Mn^{3+} stripe.

References

1. Z. Jirak, S. Krupicka, V. Nekvasil, E. Pollert, G. Villeneuve, F. Zounova, J. Magn. Magn. Mater. **15-18**, 519 (1980).
2. Z. Jirak, S. Krupicka, Z. Simsa, D. Dlouha, S. Vratislav, J. Magn. Magn. Mater. **53**, 153 (1985).
3. C. Zener, Phys. Rev. **82**, 403 (1951).
4. P.W. Anderson, H. Hasegawa, Phys. Rev. **100**, 675 (1955).
5. P.G. de Gennes, Phys. Rev. **118**, 141 (1960).
6. Y. Tomioka, A. Asamitsu, H. Kuwahara, Y. Moritomo, Y. Tokura, Phys. Rev. B **53**, 1689 (1996).
7. C.H. Chen, S.W. Cheong, Phys. Rev. Lett. **76**, 4042 (1996).
8. A. Barnabé, M. Hervieu, C. Martin, A. Maignan, B. Raveau, J. Mater. Chem. **8**, 6, 1405 (1998).
9. C.H. Chen, S.W. Cheong, H.Y. Hwang, J. Appl. Phys. **81**, 8, 4326 (1997).
10. P.G. Radaelli, D.E. Cox, M. Marezio, S.W. Cheong, P.E. Schiffer, A.P. Ramirez, Phys. Rev. Lett. **75**, 24, 4488 (1995)
11. A.P. Ramirez, P. Schiffer, S.W. Cheong, C.H. Cheong, C.H. Chen, W. Bao, T.T.M. Palstra, P.L. Gammel, D.J. Bishop and B. Zegarski, Phys. Rev. B **76**, 3188 (1996).
12. M.R. Ibarra, J.M. de Teresa, J. Blasco, P.A. Algaratel, C. Marquina, J. Garcia, J. Stankiewics, C. Ritter, Phys. Rev. B **56**, 8252 (1997).
13. K. Liu, X.W. Wu, K.H. Ahr, T. Sulchek, C.L. Chien, J.O. Xiao, Phys. Rev. B **54**, 3007 (1996).
14. O. Richard, W. Schuddinck, G. Van Tendeloo, F. Millange, M. Hervieu, V. Caignaert, B. Raveau, Acta Cryst. (in press).
15. W. Bao, J.D. Axe, C.H. Chen, S.W. Cheong, Phys. Rev. Lett. **78**, 543 (1997).
16. Y. Murakami, D. Shindo, H. Chiba, M. Kikuchi, Y. Syono, Phys. Rev. B **55**, 15043 (1997).
17. H. Chiba, M. Kikuchi, K. Kusaba, Y. Muraoka,Y. Syono, Solid State Comm. **99**, 499 (1996).
18. I.O. Troyanchuk, N.V. Samsonenko, H. Szymezak, A. Nabialek, J. Solid State Chem. **131**, 144 (1997).
19. C. Martin, A. Maignan, F. Damay, M. Hervieu, B. Raveau, J. Solid State Chem. **134**, 198 (1997).
20. A. Maignan, C. Martin, F. Damay, B. Raveau, Chem. Mater. **10**, 950 (1998).
21. A. Maignan, C. Martin, F. Damay, B. Raveau, J. Hejtmanek. Phys. Rev. B **58**, 2758 (1998).
22. A. Maignan, C. Martin, F. Damay, M. Hervieu, B. Raveau, J. Magn. Magn. Mater. **188**, 185 (1998).
23. A. Barnabé, M. Hervieu, C. Martin, A. Maignan, B. Raveau, J. Appl. Phys. **84**, 10, 5506 (1998).
24. M. Hervieu, G. Van Tendeloo, V. Caignaert, A. Maignan, B. Raveau, Phys. Rev. B **53**, 21, 14274 (1996).
25. P.G. Radaelli, D.E. Cox, M. Marezio, S.W. Cheong, Phys. Rev. B **55**, 3015 (1997).